

Supporting Information For:

Collective interactions of quantum confined excitons in halide perovskite nanocrystal superlattices

Shai Levy^{1,2}, Orr Be'er^{1,2}, Saar Shaek^{1,2}, Alexey Gorlach², Einav Scharf³,
Yonatan Ossia³, Rotem Liran³ Kobi Cohen^{1,2}, Rotem Strassberg^{1,2}, Ido
Kaminer², Uri Banin³, and Yehonadav Bekenstein^{1,2}

1 Department of Materials Science and Engineering, Technion-Israel Institute of
Technology, 32000 Haifa, Israel

2 The Solid-State Institute, Technion – Israel Institute of Technology, 32000 Haifa,
Israel

3 Institute of Chemistry and the Center for Nanoscience and Nanotechnology, The
Hebrew University of Jerusalem, 91904, Jerusalem, Israel

Additional Results

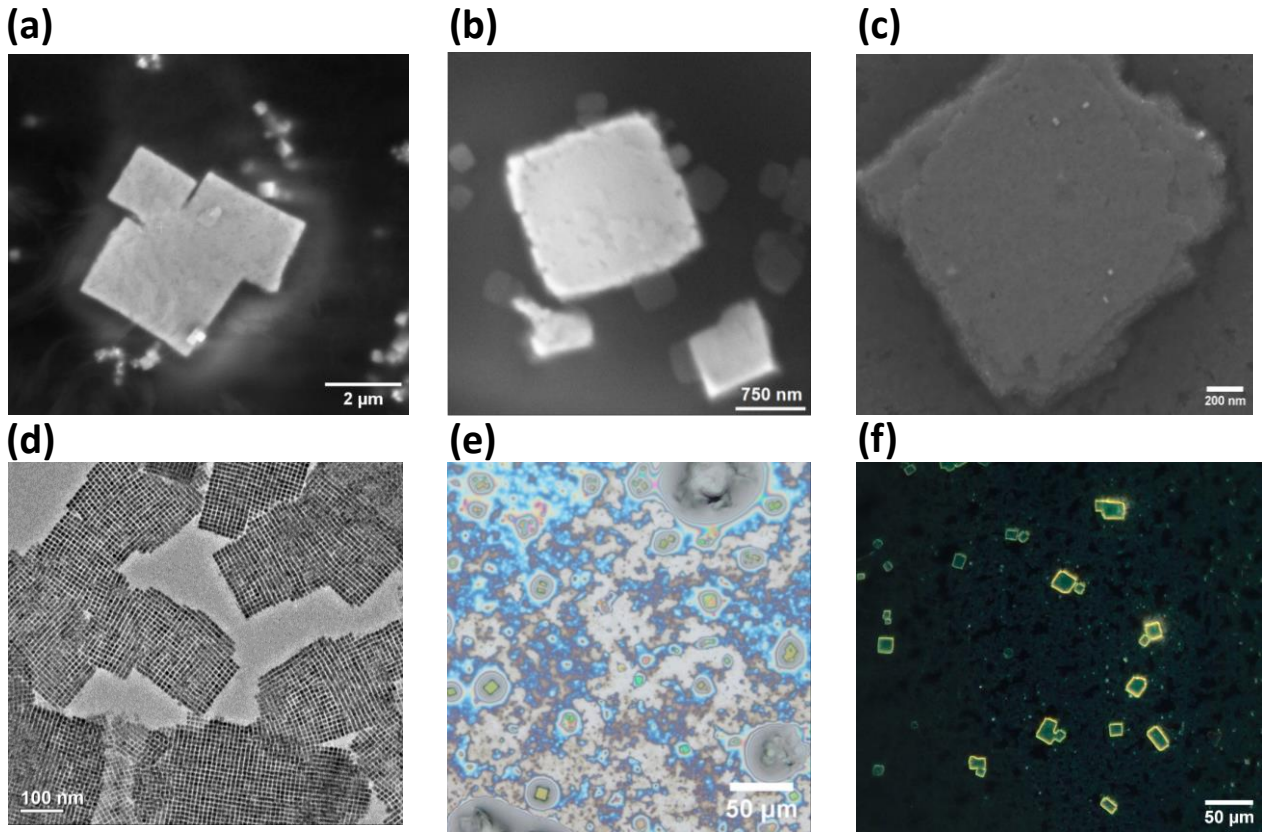


Figure S1. (a-c) SEM micrographs of rectangular CsPbBr₃ nanocrystal SLs, in (c) the surrounding colloidal glassy film is apparent. (d) Low magnification TEM micrograph of 7.8nm CsPbBr₃ nanocrystal SLs. (e-f) Optical microscope images of CsPbBr₃ nanocrystal SLs with surrounding colloidal glassy film; (e) under bright field (BF), and (f) under dark field (DF).

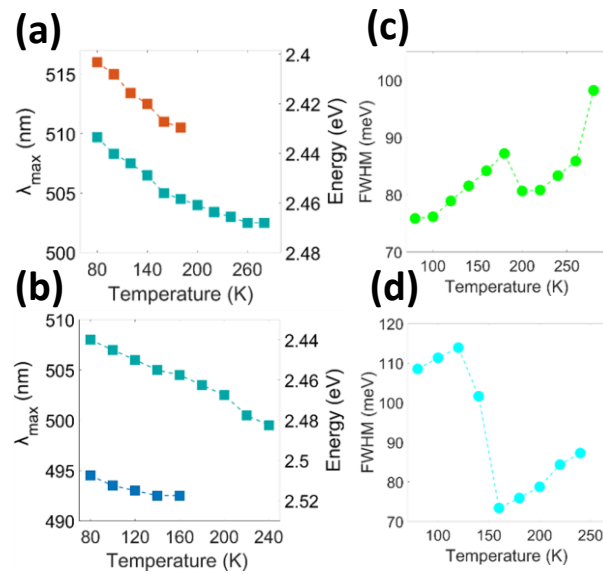


Figure S2. (a-b) peak emissions for coupled and uncoupled PL during temperature mappings of SLs made from (a) 7.8nm, and (b) 6.3nm CsPbBr₃ NCs. (c-d) Full width half maximum of PL spectra during temperature mappings of SLs made from (c) 7.8nm, and (d) 6.3nm CsPbBr₃ NCs. These plots show the coupled emission band forming below the critical temperature increasing the spectra width.

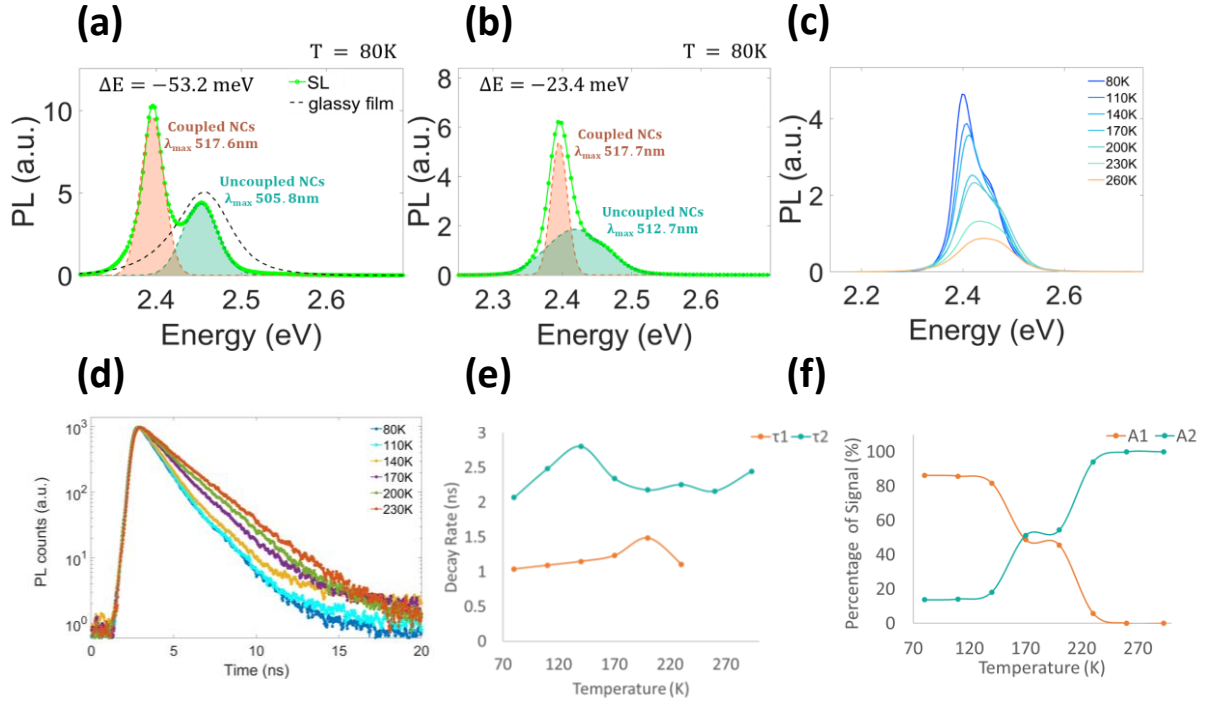


Figure S3. (a-b) Additional J aggregate behavior of weakly confined 7.8nm CsPbBr₃ nanocrystal SLs at 80K showing red-shifted PL of coupled NCs. (c) Temperature dependent PL spectra of (b). (d) TRPL at different temperatures in (c). The data matches biexponential decay for the combined coupled and uncoupled emissions. (e-f) Radiative lifetime (e), and percentage of emitted light (f) extracted from TRPL in panel (d). Below critical temp of ~200K the faster red-shifted emission appears and increases in overall intensity at lower temperatures.

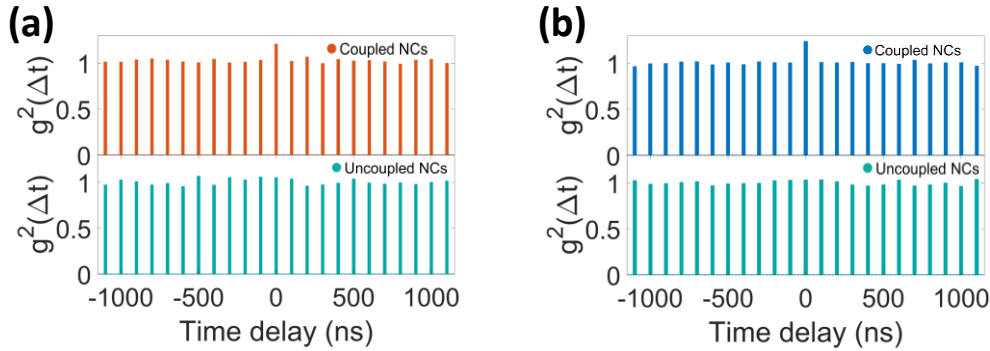


Figure S4. (a-b) Second-order correlation function measurements, obtained with a Hanbury–Brown and Twiss set-up using pulsed excitation with a 10 MHz repetition rate, and bin size of 20ns, for SLs made from (a) 7.8nm, and (b) 6.3nm CsPbBr₃ NCs. Both red-shifted and blue-shifted emission of the coupled nanocrystals show photon bunching at zero time delay, while emission of the uncoupled nanocrystals shows Poissonian photon statistics.

Liquid Helium Micro-PL:

Spectroscopic measurements at ~ 6 K were performed with a home-built microscope (DIY Cerna Components, Thorlabs). The samples were kept in a helium closed-cycle cryostat (attoDRY800, Attocube). Widefield excitation was done by 470 nm LED (EP470S10, Thorlabs) to find the regions of interest. The samples were then either excited by a pulsed laser (EPL-405, Edinburgh Instruments) at a repetition rate of 5 or 20 MHz, or a 405 nm CW laser (Wavespectrum). The lasers were focused through a cold objective (100X, 0.8 NA, Attocube), which also collected the emission. The emitted light passed through a dichroic mirror (DMLP425, Thorlabs), and a long pass filter (FELH0450, Thorlabs). The emitted light was then split with a 50:50 beamsplitter (Thorlabs) between a spectrograph (Kymera 328i, Andor) with EMCCD (iXon Ultra 888 camera, Andor), and two avalanche photodiodes (Micro Photon Devices, $100 \mu\text{m}$ PDM SPAD), with another 50:50 beamsplitter splitting the light between them. Time-stamping was performed using multichannel Time Tagger 20 (Swabian Instruments). In the lifetime measurements the spectrum was filtered to measure each peak individually (FBH500-10 and FBH520-10, Thorlabs).

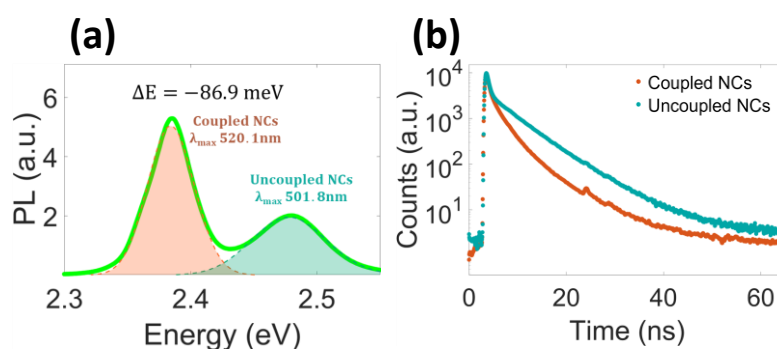


Figure S5. (a) PL spectrum at $T=6\text{K}$ of SLs made from weakly confined 7.8nm CsPbBr_3 NCs. The coupled emission is red shifted. (b) Time resolved PL at 6K of SLs made from 7.8nm CsPbBr_3 NCs. Decay rates show an accelerated red-shifted coupled emission.

Excitation Power-Dependent PL:

Excitation power dependent PL measurements were conducted at 10K using 405 nm CW diode laser. The laser beam was focused using a 20x objective with NA of 0.29 and the working distance of 31 mm, reaching a laser spot diameter of 880 nm on the cooled sample. The spectrum of the emission was measured with a TRIAX 552 spectrometer equipped with a cooled CCD (Roper Scientific). Figure S6 show excitation power dependent PL of superlattices made from 7.8nm and 6.3nm CsPbBr₃ nanocrystals. In both samples, the peak intensity of the uncoupled emission showed a linear dependency upon the excitation power as expected, without any signs of nanocrystal degradation. The coupled red-shift PL of superlattices made from 7.8nm CsPbBr₃ nanocrystals showed a super-linear behavior as expected from superfluorescence, whereas the 6.3nm sample showed a coupled blue-shift emission with a sub-linear behavior. The sublinear behavior of the collective blue-shifted emission may be the result of emitter saturation in the slower collective emission mechanism at higher power or a sign of slower emission rates due to increased excitation as shown in some subradiant systems.

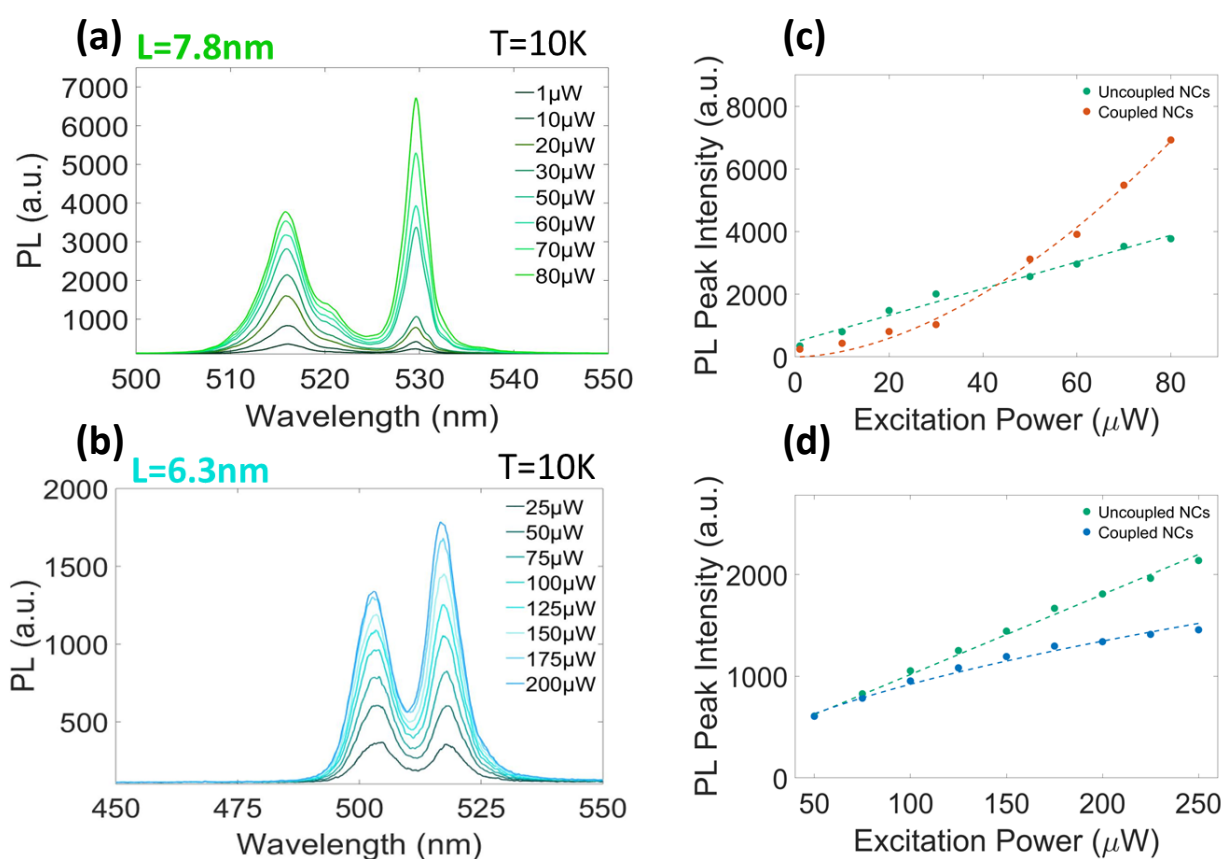


Figure S6. (a-b) Excitation power dependent PL measurements at 10K of superlattices made from (a) 7.8nm, and (b) 6.3nm CsPbBr₃ nanocrystals. (c-d) PL peak intensity of coupled and uncoupled emissions measured against excitation power of superlattices made from (c) 7.8nm, and (d) 6.3nm CsPbBr₃ nanocrystals. The PL of uncoupled NCs (green) behave linearly with the excitation power for both samples. The coupled red-shift PL at (c) show a super-linear behavior, and coupled blue-shift emission at (d) show a sub-linear behavior.

Energy Dispersive X-ray Spectroscopy (EDS)

SEM-EDS measurements for anion exchanged nanocrystals were carried out using an FEI Quanta200 microscope. Samples were placed at a 10 mm working distance and were measured at an acceleration voltage of 10 (KV). SEM-EDS measurements were calibrated by removing the substrate background signal of Silicon.

Table S1. EDS elemental composition results, excluding C, O, and Si.

I exchange			Cl exchange		
CsPb(Br _{0.6} I _{0.4}) ₃			CsPb(Br _{0.6} Cl _{0.4}) ₃		
Element	Line Type	Atomic %	Element	Line Type	Atomic %
Br	L series	6.6	Cl	K series	1.6
I	M series	4.5	Br	L series	2.5
Cs	M series	3.5	Cs	M series	1.3
Pb	M series	3.4	Pb	M series	1.3
CsPb(Br _{0.7} I _{0.3}) ₃			CsPb(Br _{0.8} Cl _{0.2}) ₃		
Element	Line Type	Atomic %	Element	Line Type	Atomic %
Br	L series	6.8	Cl	K series	0.8
I	M series	3.0	Br	L series	2.9
Cs	M series	3.3	Cs	M series	1.7
Pb	M series	3.1	Pb	M series	1.3

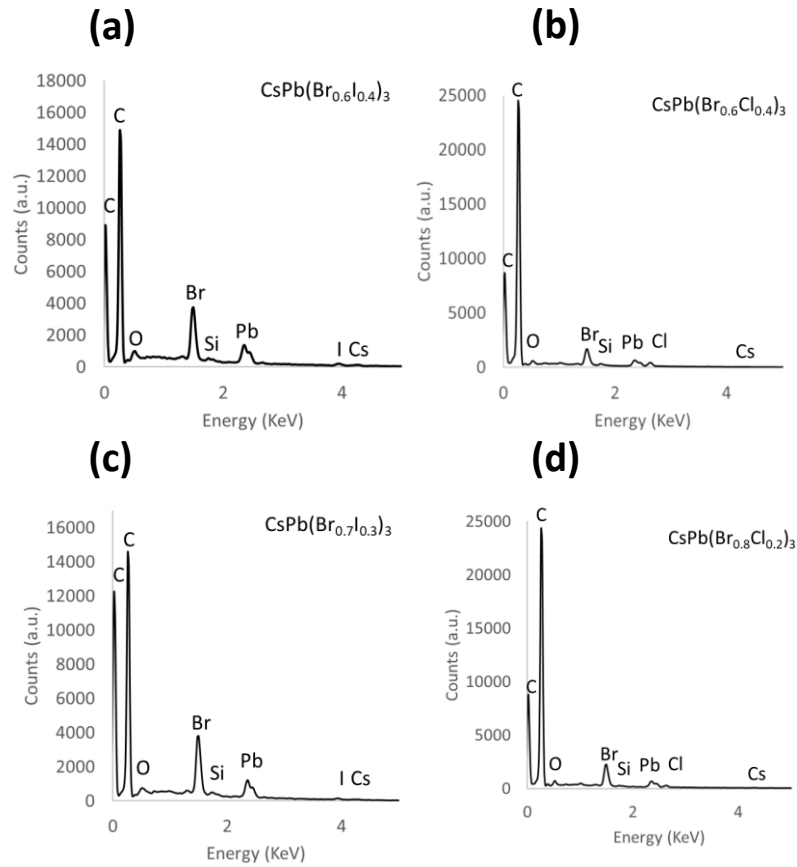


Figure S7. (a-d) EDS spectra for different samples of mixed halide from anion exchange for I exchanged (a) $\text{CsPb}(\text{Br}_{0.6}\text{I}_{0.4})_3$, and (c) $\text{CsPb}(\text{Br}_{0.7}\text{I}_{0.3})_3$. For Cl exchanges (b) $\text{CsPb}(\text{Br}_{0.6}\text{Cl}_{0.4})_3$, and (d) $\text{CsPb}(\text{Br}_{0.8}\text{Cl}_{0.2})_3$.

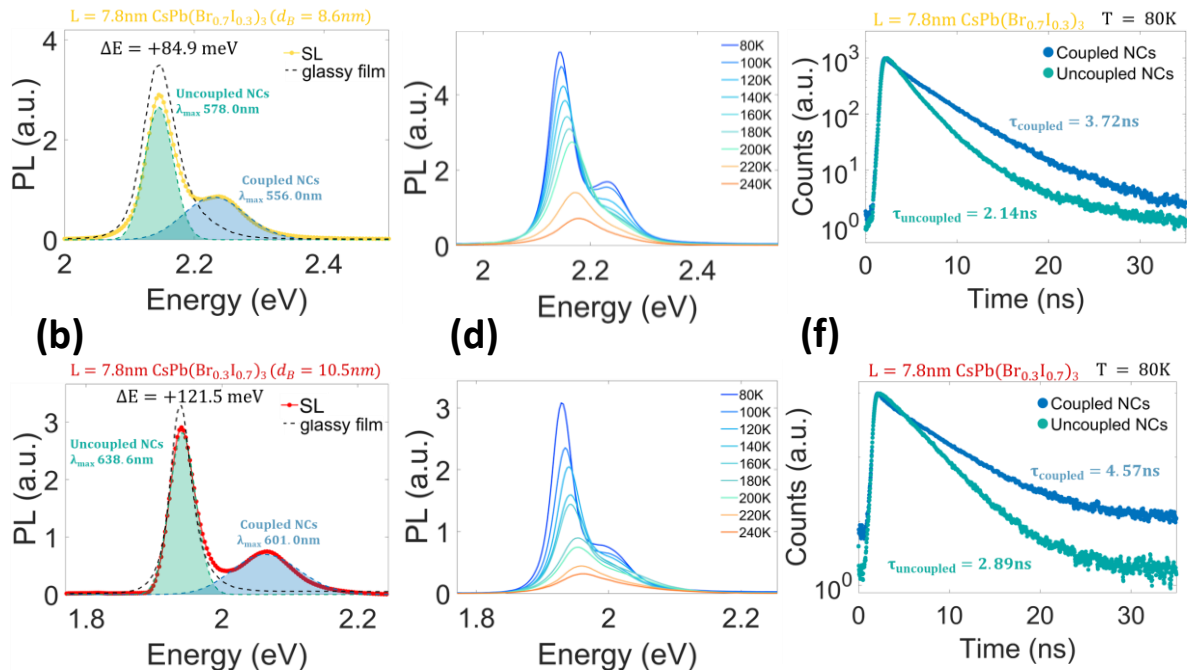


Figure S8. (a-b) PL spectrum at $T=80\text{K}$ of SLs made of anion exchanged 7.8nm (a) $\text{CsPb}(\text{Br}_{0.7}\text{I}_{0.3})_3$, and (b) $\text{CsPb}(\text{Br}_{0.3}\text{I}_{0.7})_3$ NCs. The compositional changes modify the extent of quantum confinement and reverses the spectral behaviors of native 7.8nm CsPbBr_3 nanocrystal SLs. **(c-d)** PL spectra at different temperatures of SLs made of 7.8nm (c) $\text{CsPb}(\text{Br}_{0.7}\text{I}_{0.3})_3$, and (d) $\text{CsPb}(\text{Br}_{0.3}\text{I}_{0.7})_3$ NCs. In the chemically strongly quantum confined NCs a blue-shifted band appear at cryogenic temperatures. **(e-f)** Time resolved PL of SL made of 7.8nm (e) $\text{CsPb}(\text{Br}_{0.7}\text{I}_{0.3})_3$, and (f) $\text{CsPb}(\text{Br}_{0.3}\text{I}_{0.7})_3$ NCs.

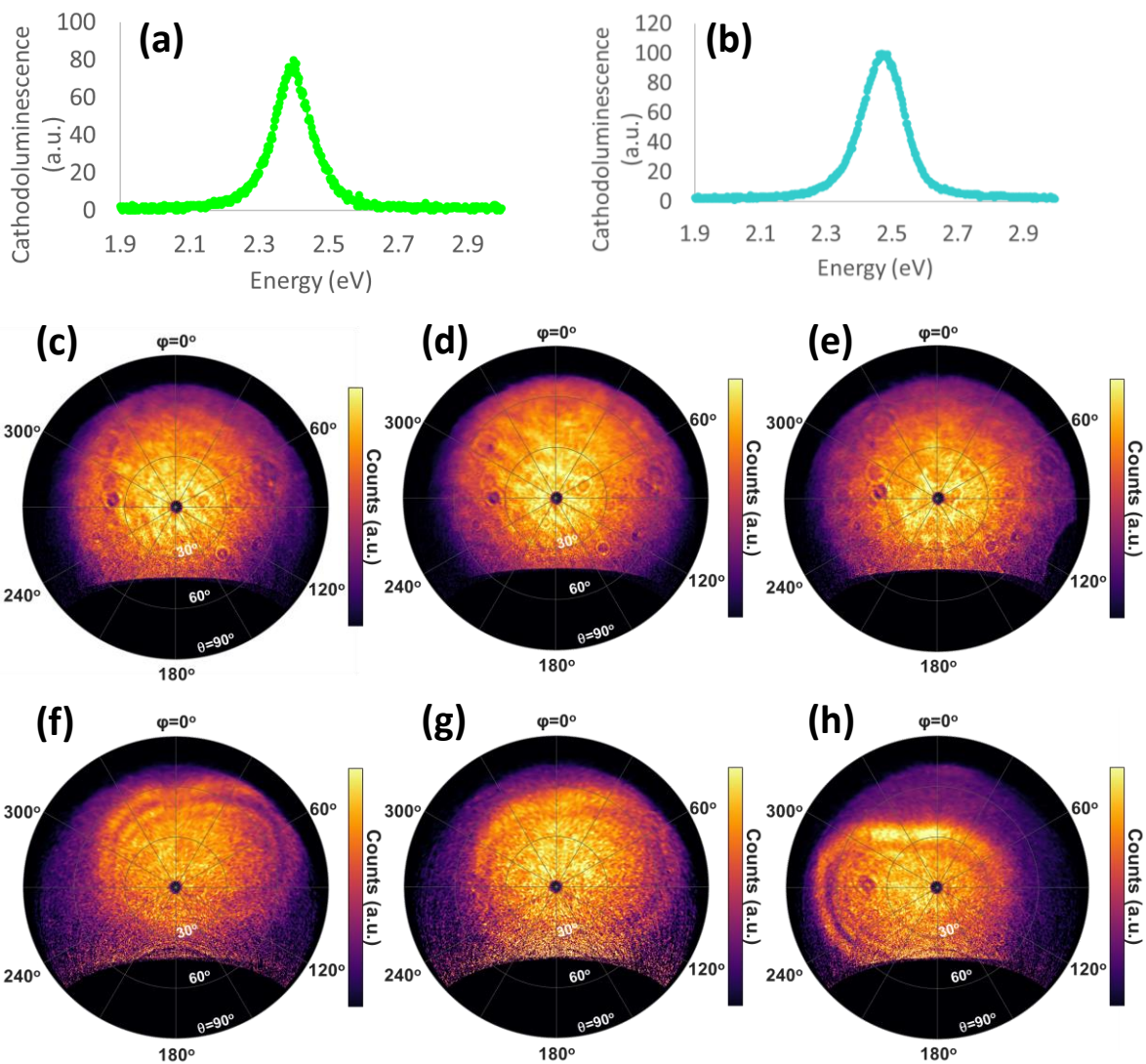


Figure S9. (a-c) CL spectra of SLs made from (a) 7.8nm, and (b) 6.3nm CsPbBr₃ NCs. (c-h) additional angular resolved CL emission patterns of SLs made from (c-e) 7.8nm, and (f-h) 6.3nm CsPbBr₃ NCs.

Exciton Energy Calculation

The energy of an exciton (E_{ex}) is given by:

$$[S1] E_{ex} = E_c + E_b$$

For E_c quantum confinement energy, and E_b binding energy. Both confinement and binding energies are dependent on the available distance in the nanocrystal, and are given by Brus equation¹:

$$[S2] E_b(d) = -\frac{1.8e^2}{2\pi\epsilon d}$$

$$[S3] E_c(d) = \frac{h^2}{8\left(\frac{d}{2}\right)^2} \left(\frac{1}{m_e^*} + \frac{1}{m_h^*} \right)$$

For h Planck constant, d the effective available distance for excitons in the nanocrystal, m_e^*/m_h^* the effective mass of electrons/holes in the semiconductor, e the electron charge, and ϵ the effective dielectric constant of the perovskite.

For $CsPbBr_3$ the effective masses were previously reported²:

$$m_e^* = 0.15m_0, m_h^* = 0.14m_0, \epsilon = 4.96\epsilon_0 \text{ for } \epsilon_0 \text{ the vacuum permittivity.}$$

Using these parameters, we can calculate the exciton confinement and binding energies for $d=7.8\text{nm}$:

$$E_c(d = 7.8\text{nm}) = \frac{(6.626 * 10^{-34})^2 \left[\text{m}^4 * \frac{\text{Kg}^2}{\text{sec}^2} \right]}{8 * 3.9^2 * 10^{-18} [\text{m}^2]} * \mu \left[\frac{1}{\text{Kg}} \right]$$

$$E_c(d = 7.8\text{nm}) = 341\text{meV}$$

$$E_b(d = 7.8\text{nm}) = -\frac{1.8 * (1.6 * 10^{-19})^2 [\text{C}^2]}{2\pi * 4.96 * 8.854 * 10^{-12} \left[\frac{\text{C}}{\text{J} * \text{m}} \right] * 7.8 * 10^{-9} [\text{m}]}$$

$$E_b(d = 7.8\text{nm}) = 133.6\text{meV}$$

In similar way we calculated the energy of excitons aligned at various inclination angles β in cuboid $CsPbBr_3$ nanocrystal along the edges/corners for different sized nanocrystals as presented in figure S10.

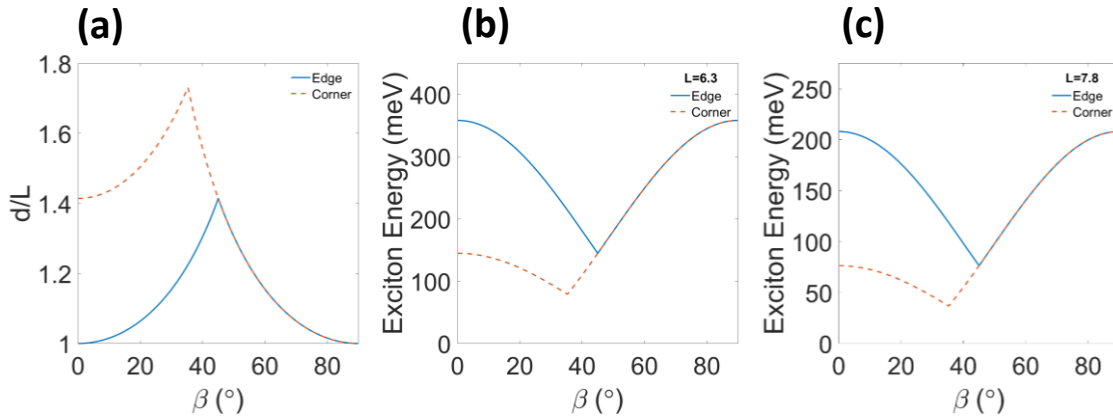


Figure S10. (a) Available effective distance in cuboid nanocrystal with edge size L for excitons aligned along the edge/corner of the nanocrystal, with inclination angle β . (b-c) Exciton energy for alignment along the edge/corner of the nanocrystal at various inclination angles in a cuboid nanocrystal with edge size (b) 6.3nm, and (c) 7.8nm.

X-Ray Diffraction (XRD):

One drop of dilute nanocrystal solution was cast on a silicon substrate for θ - 2θ temperature-dependent measurements. Measurements were taken using a Rigaku Smart-Lab 9kW high-resolution X-ray diffractometer equipped with a rotating anode X-ray source and a HyPix-3000 detector. We used a 1.54\AA ($\text{Cu K}\alpha$) wavelength and performed θ - 2θ measurements with a 2θ range of 10° - 70° with a step size of 0.01° and a temperature range of 298-140K. The in-situ cooling measurements were conducted using a temperature-dependent attachment stage with a carbon dome in a vacuum environment.

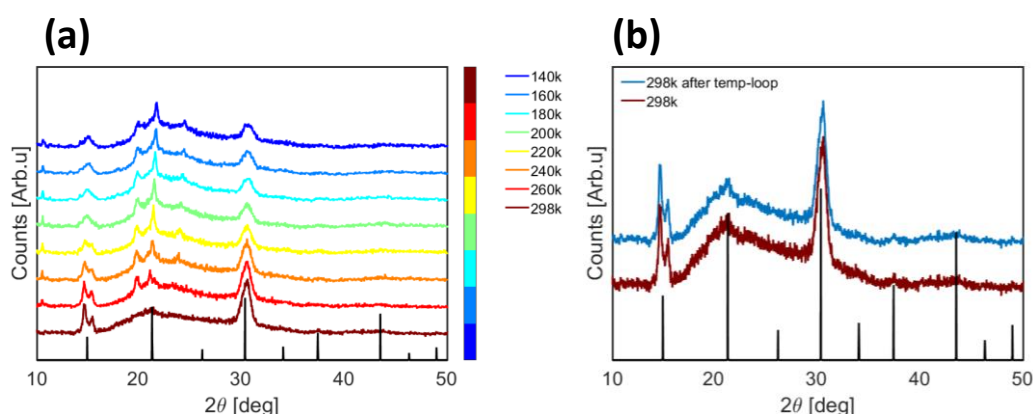


Figure S11. (a) Cryo X-ray diffractions of CsPbBr_3 nanocrystal SLs sample at different temperatures. (b) X-ray diffractions of CsPbBr_3 nanocrystal SL at 298K before and after cooling of the sample. Both panels include bulk reference ICDD no. 01-074-2251.

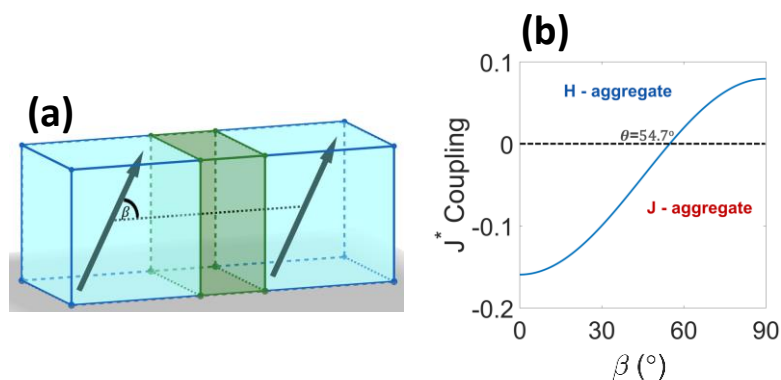


Figure S12. (a) Schematic of coupled nanocrystal dimer with coplanar transition dipole conformation. (b) Coulomb coupling conformation factor calculation for coplanar transition dipoles as a function of inclination angle β .

References:

1. Brus, L. E. Electron–electron and electron-hole interactions in small semiconductor crystallites: The size dependence of the lowest excited electronic state. *J Chem Phys* **80**, 4403–4409 (1984).
2. Protesescu, L. *et al.* Nanocrystals of Cesium Lead Halide Perovskites (CsPbX_3 , X = Cl, Br, and I): Novel Optoelectronic Materials Showing Bright Emission with Wide Color Gamut. *Nano Lett* **15**, 2023 (2015).